

Deterministic Fabrication of Liquid Metal Nanopatterns for Nanophotonics Applications

*Md Abdul Kaium Khan, Yaoli Zhao, Shreyan Datta, Puspita Paul, Shoaib Vasini, Thomas Thundat, and Peter Q. Liu**

Md Abdul Kaium Khan, Shreyan Datta, Puspita Paul, Shoaib Vasini, Peter Q. Liu

Department of Electrical Engineering, University at Buffalo, The State University of New York, Buffalo, NY 14260, USA

*E-mail: pqliu@buffalo.edu

Yaoli Zhao, Thomas Thundat

Department of Chemical and Biological Engineering, University at Buffalo, The State University of New York, Buffalo, NY 14260, USA

Keywords: liquid metal, gallium, eutectic gallium-indium, nanofabrication, nanophotonics

Abstract

Gallium-based liquid metals (LMs) have been widely used for stretchable and reconfigurable electronics thanks to their fluidic nature and excellent conductivity. These LMs possess attractive optical properties for photonics applications as well. However, due to the high surface tension of the LMs, it has been challenging to form LM nanostructures with arbitrary shapes using conventional nanofabrication techniques. As a result, LM-based nanophotonics has not been extensively explored. Here, we demonstrate a simple yet effective technique to deterministically fabricate LM nanopatterns with high yield over a large area. This technique demonstrates for the first time the capability to fabricate LM nanophotonic structures of various precisely defined shapes and sizes using two different LMs, i.e., liquid gallium and liquid eutectic gallium-indium (EGaIn) alloy. High-density arrays of LM nanopatterns with critical feature sizes down to ~100 nm and inter-pattern spacings down to ~100 nm have been achieved, corresponding to the highest resolution of any LM fabrication technique developed to date. Additionally, the LM nanopatterns demonstrate excellent long-term stability under ambient conditions. This work paves the way towards further development of a wide range of LM nanophotonics technologies and applications.

1. Introduction

Over the course of the last decade, room temperature liquid metals (LMs) have been extensively studied for their potential use in soft electronics applications, such as stretchable and reconfigurable conductors,^[1,2] wearable healthcare devices,^[3,4] sensors,^[5] and energy harvesting systems.^[6] Among all the available LMs, Ga and Ga-rich alloys have been widely used thanks to their low melting points (29.8 °C for Ga, 15.7 °C for EGaIn alloy, and 10.6 °C for Galinstan alloy), high electrical and thermal conductivities, low vapor pressure, and low toxicity.^[7-9] In most cases, the required feature sizes of these LM-based electronic devices are in the range of tens of microns to millimeters. A variety of techniques have been successfully utilized to achieve such a patterning resolution for Ga-based LMs. However, owing to the fluidic nature and high surface tension (~700 mN/m) of these LMs,^[10] it is significantly more challenging to achieve patterning resolution in the sub-micron range.^[11,12] Therefore, new techniques with the capability to pattern arbitrary LM nanostructures is highly desired, as they may enable a host of new technologies and applications in the field of LM-based nanophotonics.^[13]

Most of the conventional techniques for fabricating nanostructures made of solid materials are not suitable for patterning LMs due to the inherent fluidic nature and high surface tension of LMs. For example, the physical vapor deposition techniques do not result in LM thin films, but rather produce randomly distributed LM microparticles and nanoparticles.^[13] In recent years, several techniques including molding,^[12,14,15] micro-fluidic injection,^[16,17] stenciling,^[18-20] laser sintering and ablation,^[21-23] stamping,^[24] and selective wetting^[25-30] have been developed to pattern LM structures for various applications. Some of these techniques have shown capability to achieve LM patterns with micron scale feature sizes. For example, close to 2 μm linewidths were achieved for patterning LM lines by molding,^[12] stamping,^[24] and selective wetting.^[26-28] More recently, much efforts have been devoted to achieving sub-micron feature sizes. Notably, three different techniques were demonstrated to achieve LM lines with linewidths of hundreds of nm. Kim et al. developed a hybrid nanofabrication technique based on the combination of electron-beam lithography (EBL), stamping, and soft transfer.^[31] An et al. developed a pulsed laser lithography technique to achieve laser-induced periodic surface structures.^[32] Jung et al. proposed an elastomer-based selective filling and dewetting technique for flexible 3D interconnects by utilizing the negative osmotic pressure created by a volatile solvent.^[33] Although these techniques

demonstrated conducting LM lines with sub-micron linewidths, their relatively sophisticated processes and inherent limitations may hinder their potential utility for producing high-density arrays of nanopatterns for various nanophotonics applications.

Employing LMs in photonic structures has the appealing prospect to realize reconfigurable and self-healing photonics. LMs have been employed in the bulk form as tunable or deformable ground planes for metasurfaces and optical antennas.^[34-36] In addition, patterned LM structures have been utilized for reconfigurable microwave and terahertz metamaterials and metasurfaces.^[37-40] However, due to the lack of technique for deterministically patterning LM nanostructures, similar success has not been achieved for infrared-visible-ultraviolet (IR-Vis-UV) photonics. Liquid Ga and Ga-based alloys have been investigated for their plasmonic properties and applications,^[41-44] as liquid Ga has a high plasma frequency (~ 14.1 eV) comparable to that of Al, and the lack of interband absorption and grain boundary in LMs leads to reduced optical loss.^[45] However, these previous studies were mostly based on LM nanoparticles produced by non-deterministic processes, e.g., sonication or physical vapor deposition, which provided little control over the particle size, shape, and spatial distribution. To address this issue, Martin-Monier et al. developed a low-vacuum evaporation technique to deposit LM thin film on a surface-treated elastomer and demonstrated a mid-IR metasurface consisting of an array of LM micro-disks with ~ 1.2 μm disk diameter.^[46] However, those LM micro-disks still consisted of aggregated nanoparticles of irregular shapes and sizes rather than uniform and smooth thin film structures.

To further advance technologies and applications of LM-based nanophotonics, more effective and reliable techniques for patterning LM nanostructures with arbitrary shapes, sizes and spatial distributions are required. Here, we demonstrate a facile and reliable method to deterministically fabricate LM nanopatterns by utilizing the selective adhesion of Ga-based LMs on gold surface. We realize high-density and uniform arrays of LM nanopatterns with various shapes and dimensions, which exhibit resonant optical responses in the IR region and/or plasmonic responses in the visible region. The smallest feature size and inter-pattern spacing achieved are both close to 100 nm, representing the state-of-the-art among all LM nanofabrication techniques demonstrated to date. Additionally, our technique offers advantages such as producing LM nanopattern arrays

over a large area with high yield and minimal design offset. This work may facilitate the advancement of LM-based nanophotonics with a wide range of potential applications.

2. Results and Discussion

2.1. Nanofabrication Process

The adhesion between a liquid and a solid surface is primarily dictated by the relative surface energy difference between the two materials. The liquid wets the materials with higher surface energies and avoids the ones with lower surface energies. Exploiting this phenomenon, it is possible to make a LM selectively wet patterns made of a relatively high surface energy metal (e.g., Au, Cu, Ag) on a relatively low surface energy substrate (e.g., Si, SiO₂), which leads to intermetallic bonding at the interface between the high surface energy metal and the LM.^[28] The intermetallic bonding can lead to a much stronger adhesion between the LM and the underlying surface than the van der Waals interaction between the thin oxide skin of LM and the underlying surface.^[47] Previously, a few studies utilized this phenomenon and demonstrated LM micro-lines with linewidth down to $\sim 2 \mu\text{m}$.^[26-28] The selective wetting process was achieved by spreading LM on the substrate,^[26] spin coating LM on the substrate,^[27] or stamping the substrate onto a LM puddle.^[28] Nevertheless, these techniques have not been further developed to pattern nanoscale LM structures which may form the building blocks for a wide range of nanophotonics applications. In this work, we systematically studied various factors which may influence the selective wetting process, and identified and optimized several key parameters which led to high-fidelity and high-yield fabrication of a variety of LM nanopatterns.

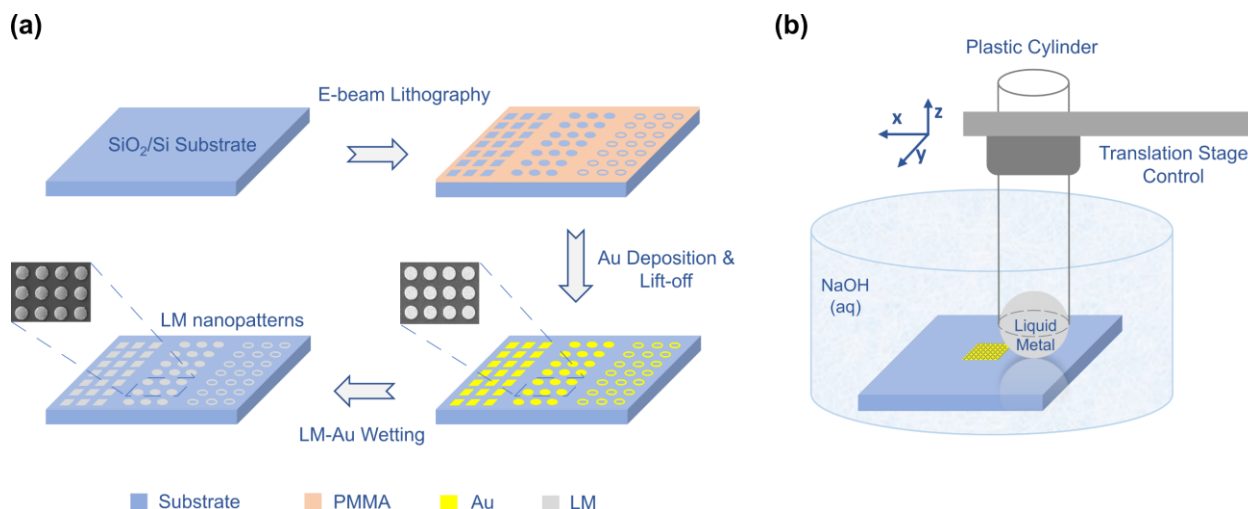


Figure 1. LM nanopattern fabrication process. a) Schematic illustration of different fabrication steps. b) Schematic depicting the setup utilized to control wetting between the LM and the Au nanopatterns on the substrate in a NaOH solution bath.

Figure 1a shows an overview of our fabrication process which involves three major steps: (1) standard nanoscale patterning using EBL or photolithography; (2) Au deposition and lift-off to form the designed Au nanopatterns; and (3) precise pattern transfer to LM utilizing the selective wetting mechanism (see Methods). The first and second steps are crucial for achieving the optimal surface profile of the Au nanopatterns, which in turn influences the wetting between the Au surface and the LM during the third step. Therefore, it is imperative to optimize the process parameters of these two critical nanofabrication steps. The electron beam dose for the EBL process is an important process parameter, as it plays a crucial role in resist development, which in turn affects the subsequent formation of Au nanopatterns after the Au deposition and lift-off. We found that when the Au nanopatterns featured thicker edges (see **Figure S1** in Supporting Information), the selective wetting process consistently produced high-quality and high-yield results. Such surface profiles of Au nanopatterns can be reliably achieved by optimizing the electron beam dose. During the second step, the deposition thickness of the Au film was optimized to be 20 nm for selective wetting with EGaIn and 10 nm for selective wetting with Ga, which led to consistent results. The quality of the LM nanopatterns is also highly sensitive to how the bulk LM droplet is rolled over the underlying Au nanopatterns. To achieve relatively precise control over this process, we constructed the setup depicted in **Figure 1b**. The setup included a narrow plastic tube for confining

a LM droplet, mounted on a translation stage with three degrees of freedom to precisely control the movement of the tube (and hence the LM droplet) on the planar substrate. A tube movement speed of approximately 100 $\mu\text{m/s}$ was found to be optimal to achieve the best selective wetting results. A photo of the setup and further descriptions can be found in **Section S2** of the Supporting Information. Prior to the selective wetting process, the samples with Au nanopatterns were cleaned using a low-power oxygen plasma treatment. The selective wetting process was conducted in a NaOH (0.3 M) solution bath to remove the naturally formed self-limiting oxide layer on the surface of the LM droplet. The surface oxide removal facilitated the direct contact between the Au nanopatterns and the LM, and suppressed potential adhesion between the LM and the substrate surface. As a result, the LM droplet only wetted the Au nanopatterns, resulting in LM nanopatterns of the exact same shapes while leaving no LM residue on the substrate surface. The samples were then taken out of the NaOH bath, rinsed thoroughly in deionized water and blown dry.

2.2. Characterizations of LM Nanopatterns

Figure 2 shows the scanning electron microscope (SEM) images of multiple densely packed liquid EGaIn nanopatterns with different shapes and sizes. Such nanopatterns are frequently used in various nanophotonic applications. These samples demonstrate the ability of our technique to achieve high-density nanopattern arrays over a large area with excellent yield. Here, we define the yield as the ratio of the number of LM nanopatterns attained after Au-LM wetting to the total number of initial Au nanopatterns. As can be clearly seen in **Figure 2**, the LM nanopatterns are faithful copies of the underlying Au nanopatterns, and no LM residue is observed on the substrate surface (SiO_2). The surfaces of these LM nanopatterns are smooth (a signature of being in the liquid phase) and do not show the granular texture of the underlying Au nanopatterns (see Supporting Information **Figure S1**). Owing to the high surface tension of LMs, LM nanoparticles tend to form spherical shapes. Therefore, we expect that LM nano-disks are relatively easier to realize than other shapes. Indeed, we were able to fabricate uniform arrays of LM nano-disks of different sizes (i.e., ~ 750 nm, ~ 500 nm, ~ 400 nm, ~ 300 nm, and ~ 200 nm in diameter) with $>99\%$ yield over an array area of $\sim 55 \times 55 \mu\text{m}^2$. **Figure 2a-b** show dense nano-disk arrays with two different nano-disk diameters, i.e., 750 nm and 200 nm, respectively. In the 200-nm nano-disk array, 24960 nano-disks were fabricated within an area of $55.7 \times 54.3 \mu\text{m}^2$, corresponding to a high density of $\sim 8.27 \times 10^6$ disks/ mm^2 . On the other hand, multiple LM nanopatterns with non-spherical

shapes were realized with high quality and yield as well. The arrays of LM nano-pentagons (**Figure 2c**), nano-squares (**Figure 2d**), nano-triangles (**Figure 2e**), and nano-hexagons (**Figure 2f**) with straight edges and sharp corners indicate that the intermetallic bonding is strong enough to effectively overcome LM's tendency of forming spherical shapes due to the high surface tension.

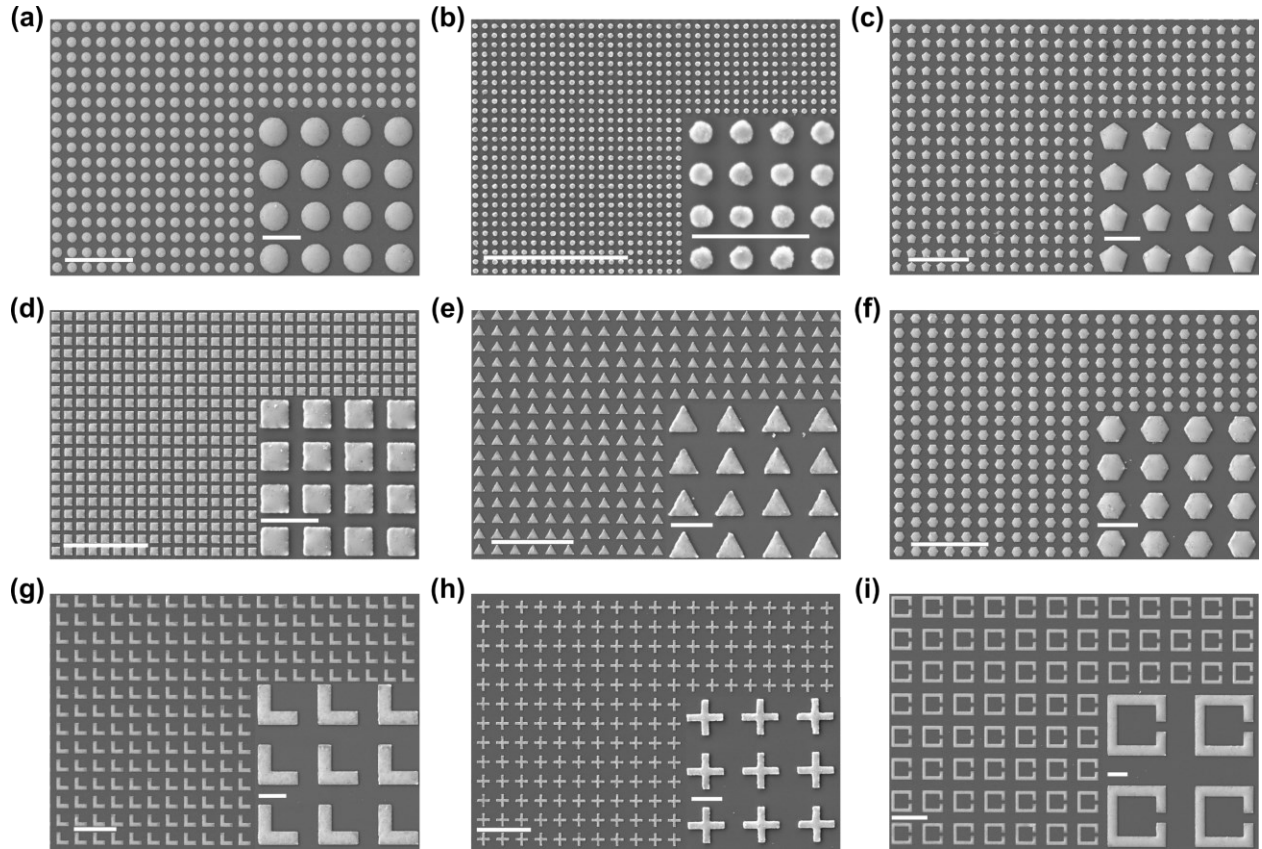


Figure 2. SEM images of fabricated liquid EGaIn nanopatterns. a-f) Densely packed arrays of various convex-shaped nanopatterns of different sizes, along with the zoomed-in images of smaller regions in the insets. g-i) Arrays of different non-convex-shaped nanopatterns, along with the zoomed-in images of smaller regions in the insets. The scale bar indicates 5 μm for the larger images and 1 μm for the inset images in all cases.

The successful realization of the various LM nanopatterns with high pattern transfer fidelity demonstrate the versatility of our deterministic LM nanofabrication technique. Most of these arrays of LM nanopatterns with convex shapes achieved ~ 98 -100% yield (see Supporting Information **Figure S3** and **Section S3**). Our technique is also capable of realizing even smaller

LM nanopatterns. **Figure S4** (see Supporting Information) shows the SEM images of several LM nanopattern arrays with sub-150 nm critical feature sizes. The quality and yield of these sub-150 nm LM nanopatterns are currently lower than the larger ones, which are mainly limited by our EBL-based process for fabricating the Au nanopatterns, rather than by the selective wetting process. With further optimization of the nanofabrication process, we expect that it will be feasible to achieve high-quality and high-yield fabrication of sub-150 nm or even sub-100 nm LM nanopatterns, which can support localized surface plasmon resonances in the UV region.

We further investigated several non-convex shapes which exhibit higher geometric complexity and are frequently employed as nanophotonic structures. Generally, non-convex shapes in the liquid phase are more challenging to form than convex shapes, especially when the liquid possesses high surface tension. Nevertheless, as illustrated in **Figure 2g-i**, the intermetallic bonding between the LM (EGaIn) and Au is robust enough to facilitate the high-fidelity and high-yield formation of large arrays of non-convex LM nanopatterns with excellent surface profiles. The L-shaped LM nanopatterns in Figure 2g and the LM split-rings in Figure 2i have critical feature sizes of ~ 500 nm, whereas the LM nano-crosses in Figure 2h have a critical feature size of ~ 250 nm.

In addition to liquid EGaIn nanopatterns, we also applied our selective wetting technique to produce liquid Ga nanopatterns. **Figure 3** displays the SEM images of various liquid Ga nanopattern arrays, which indicate that our technique has similar capabilities for producing high-quality nanopatterns based on both types of LMs. However, currently the yield for liquid Ga nanopatterns is slightly lower than their EGaIn counterparts. For instance, for identical array sizes, we achieved a yield of $\sim 95\%$ for Ga nano-pentagon array and $\sim 92\%$ for Ga nano-triangle array, whereas the yield for EGaIn nano-pentagon and nano-triangle arrays was $\sim 100\%$ and $\sim 98\%$, respectively. A similar trend in yield was observed for non-convex shapes as well. For example, the L-shaped Ga nanopatterns achieved a yield of $\sim 98\%$, which is slightly lower compared to a yield of $\sim 100\%$ for its EGaIn counterpart (see Supporting Information **Figure S3c-d**). We surmise that this difference may be related to the higher melting point and/or higher surface tension of liquid Ga compared to liquid EGaIn.

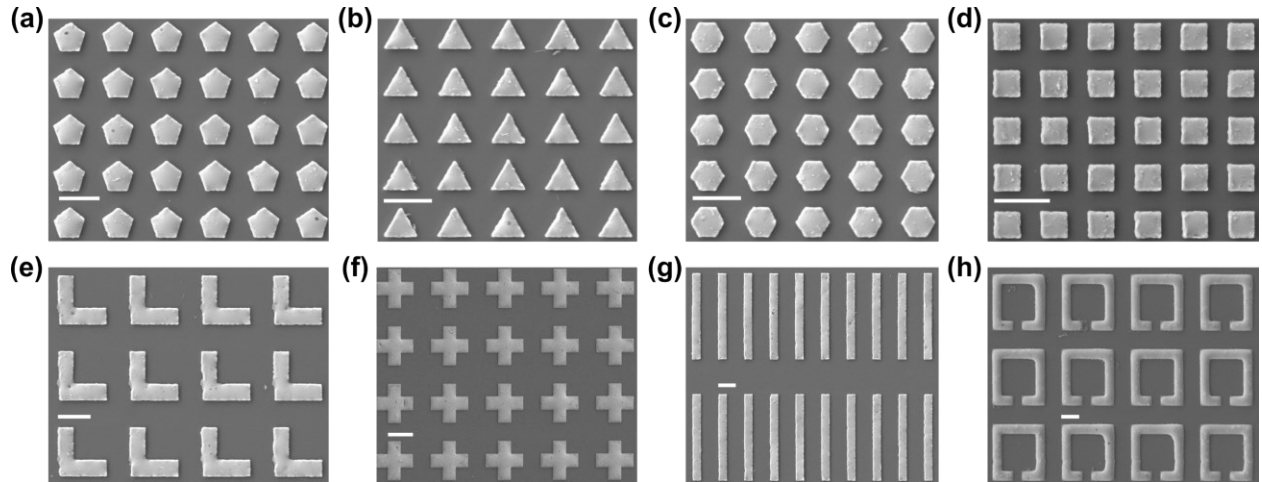


Figure 3. SEM images of liquid Ga nanopatterns. a-d) Nanopattern arrays with various convex shapes and sizes. e-h) Nanopattern arrays with different non-convex shapes and sizes. The scale bar indicates 1 μm for all images.

The surface topography of the fabricated LM nanopatterns was characterized using atomic force microscopy (AFM). **Figure 4a-b** show the 3D AFM height images and the corresponding line profiles of a liquid EGaIn nano-disk array and a liquid Ga nano-hexagon array over large scanning areas. As is typical for any liquid with high surface tension, the surfaces of the LM nanopatterns exhibit curved profiles. Across all types of LM nanostructures fabricated, the pattern thicknesses range from ~ 50 nm to ~ 200 nm, with variations attributed to differences in pattern size, shape, and process parameters. For each nano-pattern array, the thickness values of individual array elements are normally distributed with a standard deviation of < 10 nm. **Figure 4c** indicates that the thickness of a LM nanopattern exhibits a dependence on its lateral size. For identical shapes and process parameters, the LM nanopatterns become thinner with decreasing lateral size, which is consistent with the observations in previous reports.^[27,28] We observed that the LM nanopattern thickness can also be tailored by tuning certain fabrication process parameters. For example, **Figure 4d** shows that different electron beam doses of the EBL process led to different thicknesses of identical LM nanopatterns. This indicates that the surface profile of the Au nanopattern (which is sensitive to the electron beam dose as discussed in the previous section) has a significant influence on the LM nanopattern thickness.

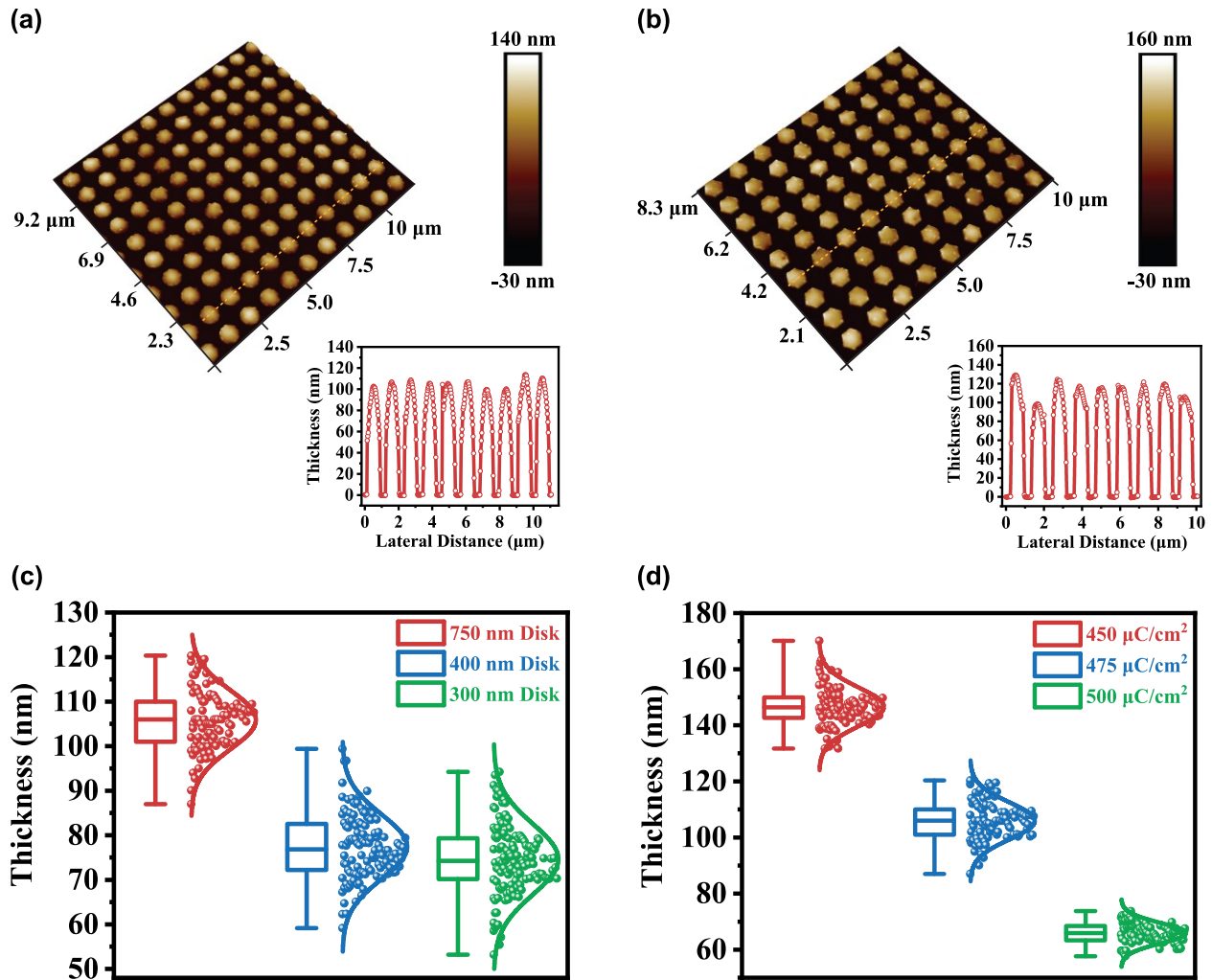


Figure 4. AFM characterization of the surface topography of fabricated LM nanopatterns. a) Top: 3D AFM image of a liquid EGaIn nano-disk array. Bottom: Line profile along the dashed line indicated in the 3D image. b) Top: 3D AFM image of a liquid Ga nano-hexagon array. Bottom: Line profile along the dashed line indicated in the 3D image. c) Thickness distributions for EGaIn nano-disks of different disk diameters. d) Thickness distributions for 750 nm EGaIn nano-disks fabricated with different electron beam doses. For (c-d), the boxes range from 25th percentile to 75th percentile with a median line, and the whiskers represent the minimum and maximum data.

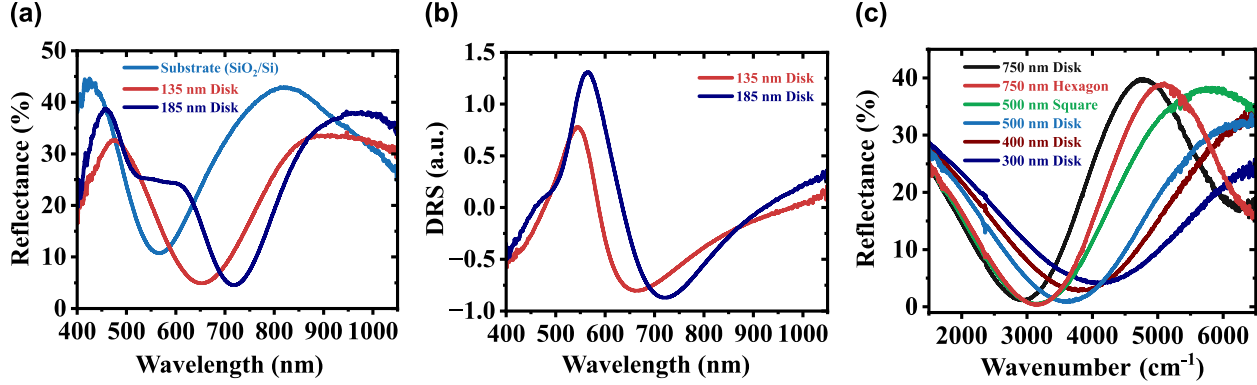


Figure 5. Reflectance spectra of different arrays of liquid EGaIn nanopatterns. a) Reflectance spectra of two nano-disk arrays within the visible to near-IR spectral region in comparison to the substrate reflectance spectrum. b) Differential reflectance spectra (DRS) of the two nano-disk arrays extracted from (a). c) Reflectance spectra of 6 different nanopattern arrays within the mid-IR to near-IR spectral region.

We further characterized the spectral responses of the fabricated LM nanopattern arrays in the IR and visible spectral regions. **Figure 5a** shows the reflectance spectra of two liquid EGaIn nano-disk arrays in comparison to that of the substrate in the visible to near-IR spectral region (see Methods), and **Figure 5b** shows the corresponding differential reflectance spectra (DRS) (see Supporting Information **Section 5**). The reflectance spectrum of the Si/SiO₂ substrate is not flat but has strong spectral features owing to the Fabry-Perot resonances of the 300 nm thick SiO₂ layer, whereas the reflectance spectra of the localized plasmonic resonances of the LM nano-disks are modulated by the spectral features of the substrate. Therefore, the DRS in **Figure 5b** more clearly reveal the inherent spectral responses of the LM nanopatterns, i.e., the reflectance peaks associated with the localized plasmonic resonances. These spectral features are well reproduced by simulation (see Supporting Information **Figure S5a-b**). As the LM nanopatterns have uniform sizes, their plasmonic resonances are significantly narrower than those observed from ensembles of LM nanoparticles with random sizes and spatial locations.^[48] Owing to the high plasma frequency of liquid Ga and liquid EGaIn, these LM nanopatterns can support localized plasmonic resonances in both visible and UV regions. The observed resonance in each spectrum in **Figure 5b** is attributed to the longitudinal (in-plane) plasmonic resonance of the LM nano-disks, and we anticipate that for the structures with a thickness of ~ 150 nm and below, a transverse (out-of-plane)

plasmonic resonance is present in the UV region.^[48] Although our current spectrometer has a limited spectral range (i.e., 400 – 1050 nm) which prevents us from demonstrating UV plasmonic response for the structures fabricated here, we expect that by further reducing the lateral dimensions of the LM nanopatterns to sub-100 nm scale, both the longitudinal and transverse plasmonic resonances should reside in the UV region. On the other hand, the arrays of LM nanopatterns with relatively large lateral dimensions exhibit strong spectral responses in the mid-IR to near-IR spectral region, as can be clearly seen in the reflectance spectra in **Figure 5c**, which were measured using a Fourier transform infrared spectrometer (FTIR) (see Methods).

2.3. Stability of LM Nanopatterns

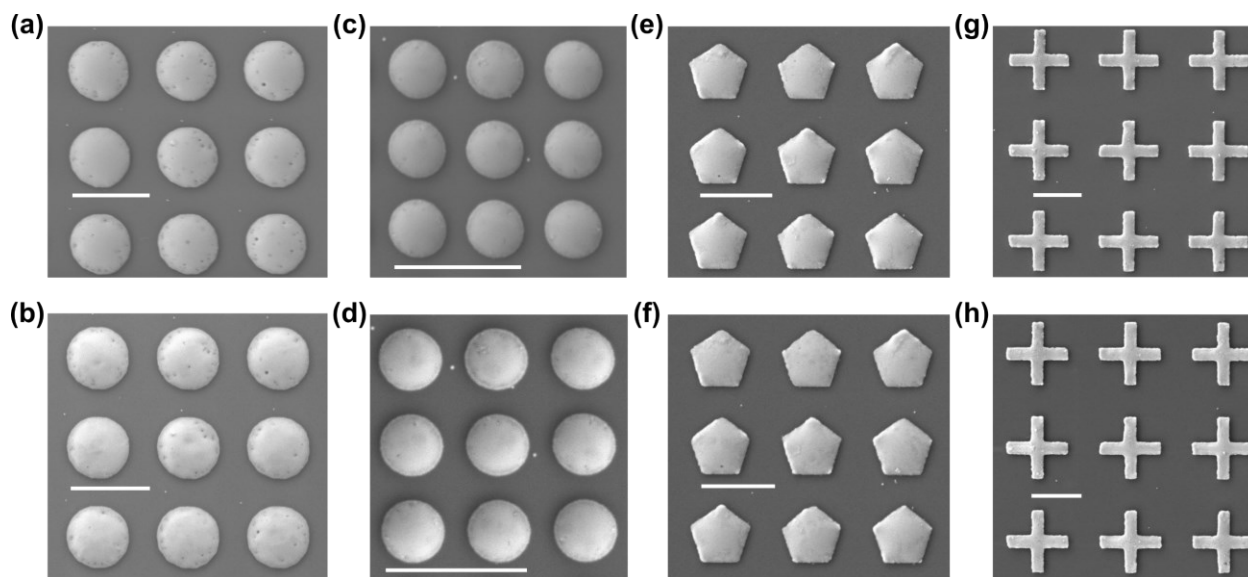


Figure 6. SEM images of several liquid EGaIn nanopattern arrays kept in ambient conditions over the course of multiple months. a) 750 nm nano-disk array at Week 1. b) 750 nm nano-disk array at Week 42. c) 400 nm nano-disk array at Week 1. d) 400 nm nano-disk array at Week 36. e) Nano-pentagon array at Week 1. f) Nano-pentagon array at Week 10. g) Nano-cross array at Week 1. h) Nano-cross array at Week 10. The scale bar indicates 1 μm for all images.

The long-term stability of the LM nanopatterns stored in ambient conditions was studied over several months. The surface profiles of the LM nanopatterns showed no observable change after several months, as evidenced by the SEM images in **Figure 6**. For instance, the SEM image of the ~ 750 nm EGaIn nano-disk array in **Figure 6b** was captured after the sample had been kept in

ambient conditions for 42 weeks, which shows no significant surface modification compared to the SEM image in **Figure 6a** taken within one week after the sample was fabricated. The ~ 400 nm nano-disk array were fabricated later and kept in ambient conditions for 36 weeks before the second SEM images were taken (see **Figure 6c** and **Figure 6d**). The observed long-term stability may be attributed to the naturally formed self-limiting surface gallium oxide layer, typically a few nm thick. The surface oxide layer protects the LM nanopatterns from degradation, such as further oxidation, over time in ambient conditions.^[47] Similar stability was observed for the other convex-shaped and non-convex-shaped LM nanopatterns, which were fabricated several months later than the aforementioned nano-disks. **Figure 6f** and **Figure 6h** show the surface profiles of nanopentagon and nano-cross arrays, respectively, after 10 weeks of ambient storage. Compared to their images from Week 1 (**Figure 6e** and **Figure 6g**, respectively), there is barely any observable change in these nanopatterns after 10 weeks, which suggests excellent long-term stability.

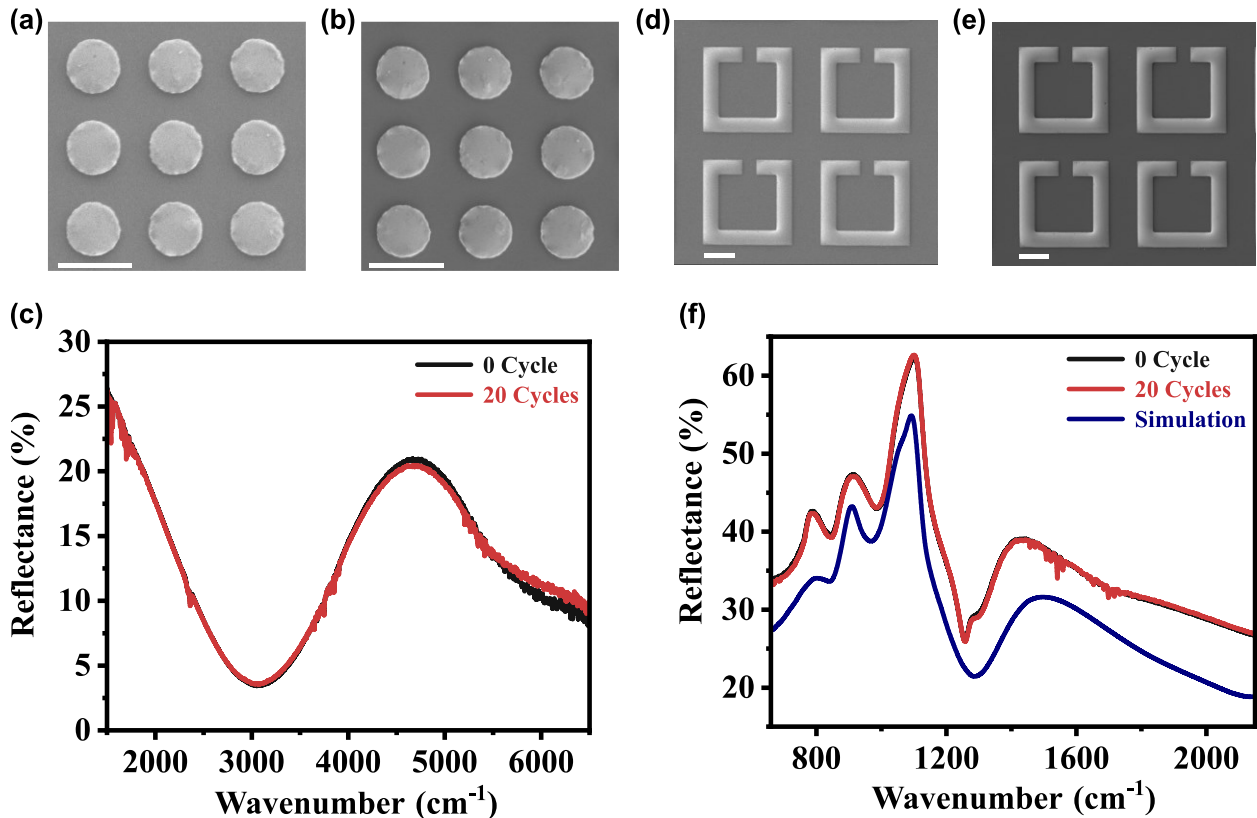


Figure 7. SEM images and reflectance spectra of liquid Ga and EGaIn nanopatterns before and after 20 cycles of temperature variation between 80 K and 313 K. a) SEM image of a liquid Ga nano-disk array at the initial stage (zero cycle). b) SEM image of the sample in (a) after 20

temperature cycles. c) Reflectance spectra of the sample in (a) and (b) before and after the 20 temperature cycles. d) SEM image of a liquid EGaIn split-ring resonator array at the initial stage (zero cycle). e) SEM image of the sample in (d) after 20 temperature cycles. f) Reflectance spectra of the sample in (d) and (e) before and after the 20 temperature cycles (the two spectra almost completely overlap) in comparison to the simulated spectrum. The scale bar indicates 1 μm for all.

The fabricated LM nanopatterns also exhibit excellent stability over large temperature variations and liquid-solid phase transitions. As the liquid-solid phase transition of Ga or EGaIn is accompanied by a large permittivity change, inducing the phase transition is an effective method to realize tunable photonic devices based on these metals.^[49] As depicted in **Figure 7**, the samples underwent 20 cycles of temperature variation, ranging from 80 K to 313 K in a cryostat, before being characterized at room temperature. Each cycle involved two phase transitions, from liquid to solid and from solid to liquid again, resulting in a total of 40 phase transitions. Note that the Ga and EGaIn nanopatterns are expected to be in the solid phase at low cryogenic temperatures such as 80 K,^[50,51] although our instruments do not allow direct observation of their phase transition. For all the investigated samples (either Ga or EGaIn), the pattern surfaces retained their original profiles once the samples were brought back to room temperature from 80 K. For example, the comparison between **Figure 7a** and **Figure 7b** indicates that no significant change of the liquid Ga nano-disks took place after 20 temperature cycles. The reflectance spectra measured before and after the 20 temperature cycles show excellent agreement (**Figure 7c**). Similar stability was observed for the liquid EGaIn nanopatterns as well. **Figure 7d-e** show no sign of surface modification to the liquid EGaIn split-rings as a result of the 20 temperature cycles, and the spectral responses shown in **Figure 7f** are also identical in both cases. Note that the multiple reflectance peaks and valleys in the 800 to 1200 cm^{-1} wavenumber range are the result of the split-ring LC resonance coupling to the optical phonons of the underlying 300 nm thick SiO_2 layer.^[52] These spectral features are well reproduced by simulation (see Methods).

2.4. Discussion

While the demonstrated technique achieves high-yield fabrication of LM nanopatterns with approximately 150 nm feature sizes and a relatively low yield for ~ 100 nm patterns (**Figure S4**), a more comprehensive investigation into the key factors of the selective wetting process may

eventually lead to the realization of large arrays of sub-100 nm LM nanopatterns of arbitrary shapes. In addition, the Au nanopatterns for the selective wetting process can be replaced by nanopatterns made of other solid metals which can also form intermetallic compounds with Ga-based LMs.^[53-55] Although the wetting phenomenon in the nanoscale is often more complex than in macroscopic scales, the adhesion energy between LMs and intermetallic compounds (formed at the interface between LMs and various solid metals) is found to be an order of magnitude larger than the surface energy of LMs,^[54,55] which may be strong enough to overcome various effects that can inhibit wetting more significantly in the nanoscale (e.g., impurities, surface heterogeneity, line tension and thermal fluctuation). Therefore, we believe that achieving high-yield fabrication of sub-100 nm LM nanopatterns by further optimizing the selective wetting process is feasible. Several potentially viable optimizations can be explored. For example, the surface roughness of the Au nanopatterns may be tailored to promote wetting in the Wenzel regime and avoid the Cassie-Baxter regime.^[56] The edge profiles of the Au nanopatterns may be further optimized to strengthen the pinning of the LM during the selective wetting process. Furthermore, the Au or other solid metal nanopattern surface may be chemically treated to facilitate the formation of intermetallic compounds which promote the subsequent wetting with LMs.^[57]

The thickness of the Au is another important factor that needs to be carefully optimized, as part of the LM is consumed to form intermetallic compounds with Au (predominantly AuGa₂ and AuIn₂, but other stoichiometries may also be present) which enhance the LM wetting.^[58] We occasionally observed that after the selective wetting process using liquid Ga, the nanopatterns appear to be completely solid structures with granular textures, as shown in **Figure S6** (see Supporting Information), which are likely the intermetallic Au-Ga compounds formed during and after the selective wetting process.^[58] We found that this issue can be effectively mitigated by reducing the Au thickness from 20 nm to 10 nm, which in turn reduces the amount of liquid Ga that can be consumed to form the intermetallic compounds with Au. Nevertheless, future investigation is needed to fully understand how to precisely control the formation of intermetallic compounds.

3. Conclusion

We have experimentally demonstrated the feasibility of deterministic fabrication of LM-based nanophotonic structures with excellent quality and yield. The developed selective wetting-based

technique is suitable for utilizing both EGaIn and Ga to produce LM nanopatterns with various shapes and sizes, which have optical responses across the IR to visible spectral range. The smallest LM nanopatterns demonstrated have ~ 100 nm lateral dimensions with ~ 100 nm inter-pattern spacings. The LM nanopatterns have excellent long-term stability in ambient conditions, showing no sign of surface degradation over multiple months. Additionally, the LM nanopatterns exhibit robustness to multiple cycles of liquid-solid phase transitions induced by cryogenic cooling. We believe that high-yield fabrication of LM nanopatterns with sub-100 nm feature sizes may be achieved by further optimization of the process parameters. This work paves the way for future development of precisely designed LM nanophotonic structures for various applications, including tunable optical antennas and metasurfaces, as well as UV plasmonics.

4. Methods

Fabrication of Au nanopatterns: The SiO₂/Si substrates underwent a thorough cleaning process with acetone/isopropyl alcohol (IPA), followed by drying using a N₂ gun and heating on a hot plate (180 °C) for one minute to evaporate any remaining liquids from the substrate surface. Subsequently, an oxygen plasma treatment was conducted in a RIE chamber to further clean the surface. Next, a bilayer electron-beam resist was spin-coated to achieve a total thickness of ~ 260 nm. The bottom layer comprised ~ 180 nm of MicroChem 495 PMMA A4 resist, while the top layer consisted of ~ 80 nm of MicroChem 950 PMMA A2 resist. Each resist layer was spin-coated at 4000 rpm for 40 seconds and baked at 180 °C for 2 minutes. Patterning with EBL was performed using an Elionix ELS G-100 system with a 100 kV accelerating voltage. An electron beam dose of $450\text{-}600 \mu\text{C}/\text{cm}^2$ was applied for patterns of various shapes and sizes, with a 1 nA beam current. Following the exposure, the patterns were developed in a methyl isobutyl ketone/IPA (1:3) mixture for 50 seconds, followed by 10 seconds in IPA and a brief rinse in DI water. Subsequently, another round of oxygen plasma treatment was conducted in the RIE chamber to clean the developed patterns before the metal deposition. A 10 nm layer of Cr and a 10-20 nm layer of Au were deposited at a rate of $1 \text{ \AA}/\text{s}$ using an electron-beam evaporator. Finally, lift-off was performed in acetone to form the nanopatterns.

Spectral Characterization: We used an IR microscope connected to a Bruker Vertex 70v FTIR to measure the mid-IR to near-IR reflectance spectra of all samples in ambient conditions. The IR

light from the globar in the FTIR was focused on each LM nanopattern array by the IR microscope using a reflective objective (15X, 0.58 NA). Reference reflectance spectra were obtained from a flat gold mirror. Each measurement had a spectral resolution of 4 cm^{-1} and a scanning time of 5 minutes (approximately 700 scans). For measuring the reflectance spectra in the visible to near-IR spectral region, we used a home-built microscope setup connected to an Ocean Optics USB 2000 spectrograph. A stabilized tungsten-halogen light source (Thorlabs SLS201L) provided broadband light, focused on each LM nanopattern array by a Nikon objective (40X, 0.65 NA). Each measurement had a wavelength resolution of approximately 2 nm, 100 ms integration time per scan, and 50 scans.

Simulation: We utilized Ansys Lumerical FDTD to simulate the optical responses of various LM nanopatterns. In our simulation model, the substrate surface was oriented in the x-y plane. We applied periodic boundary conditions for the x- and y-boundaries and perfectly matched layer boundary conditions for the z-boundaries. The thickness of each LM nanopattern were set to the average value of its measured thickness distribution. The Drude model was used for describing the LM permittivity functions with the plasma frequency of $\omega_p = 2.123 \times 10^{16}\text{ rad/s}$ and the scattering rate of $\gamma = 1.29 \times 10^{15}\text{ s}^{-1}$.

Supporting Information

Supporting Information is available from the Wiley Online Library or from the author.

Acknowledgments

This work is in part supported by the National Science Foundation (NSF Award No. ECCS-1847203 and ECCS-1919798).

References

- [1] M. D. Dickey, *Advanced Materials* **2017**, 29, 1606425.
- [2] T. Q. Trung, N. E. Lee, *Advanced Materials* **2017**, 29, 1603167.
- [3] Y. G. Park, G. Y. Lee, J. Jang, S. M. Yun, E. Kim, J. U. Park, *Advanced Healthcare Materials* **2021**, 10, 2002280.
- [4] Y. Liu, M. Pharr, G. A. Salvatore, *ACS Nano* **2017**, 11, 9614.

- [5] M. Baharfar, K. Kalantar-Zadeh, *ACS Sensors* **2022**, 7, 386.
- [6] V. Vallem, Y. Sargolzaeiaval, M. Ozturk, Y. C. Lai, M. D. Dickey, *Advanced Materials* **2021**, 33, 2004832.
- [7] V. Y. Prokhorenko, V. V. Roshchupkin, M. A. Pokrasin, S. Prokhorenko, V. Kotov, *High Temperature* **2000**, 38, 954.
- [8] M. Pokorny, H. Astrom, *Journal of Physics F: Metal Physics* **1976**, 6, 559.
- [9] C. R. Chitambar, *International Journal of Environmental Research and Public Health* **2010**, 7, 2337.
- [10] S. Hardy, *Journal of Crystal Growth* **1985**, 71, 602.
- [11] R. K. Kramer, C. Majidi, R. J. Wood, *Advanced Functional Materials* **2013**, 23, 5292.
- [12] B. A. Gozen, A. Tabatabai, O. B. Ozdoganlar, C. Majidi, *Advanced Materials* **2014**, 26, 5211.
- [13] P. Q. Liu, X. Miao, S. Datta, *Optical Materials Express* **2023**, 13, 699.
- [14] S. H. Jeong, A. Hagman, K. Hjort, M. Jobs, J. Sundqvist, Z. Wu, *Lab on a Chip* **2012**, 12, 4657.
- [15] M. D. Dickey, R. C. Chiechi, R. J. Larsen, E. A. Weiss, D. A. Weitz, G. M. Whitesides, *Advanced Functional Materials* **2008**, 18, 1097.
- [16] Y. Lin, O. Gordon, M. R. Khan, N. Vasquez, J. Genzer, M. D. Dickey, *Lab on a Chip* **2017**, 17, 3043.
- [17] Y. Gao, H. Ota, E. W. Schaler, K. Chen, A. Zhao, W. Gao, H. M. Fahad, Y. Leng, A. Zheng, F. Xiong, *Advanced Materials* **2017**, 29, 1701985.
- [18] N. Lazarus, S. S. Bedair, I. M. Kierzewski, *ACS Applied Materials & Interfaces* **2017**, 9, 1178.
- [19] T. V. Neumann, B. Kara, Y. Sargolzaeiaval, S. Im, J. Ma, J. Yang, M. C. Ozturk, M. D. Dickey, *Micromachines* **2021**, 12, 146.
- [20] T. H. Park, J. H. Kim, S. Seo, *Advanced Functional Materials* **2020**, 30, 2003694.
- [21] S. Liu, S. N. Reed, M. J. Higgins, M. S. Titus, R. Kramer-Bottiglio, *Nanoscale* **2019**, 11, 17615.
- [22] S. Liu, M. C. Yuen, E. L. White, J. W. Boley, B. Deng, G. J. Cheng, R. Kramer-Bottiglio, *ACS Applied Materials & Interfaces* **2018**, 10, 28232.

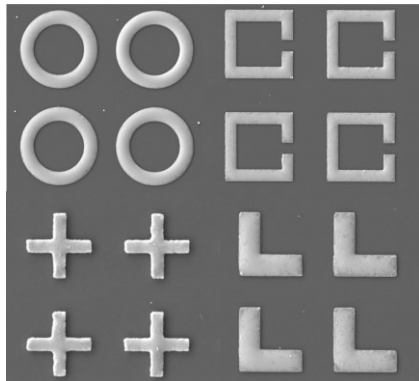
- [23] C. Pan, K. Kumar, J. Li, E. J. Markvicka, P. R. Herman, C. Majidi, *Advanced Materials* **2018**, 30, 1706937.
- [24] M. Kim, C. Kim, H. Alrowais, O. Brand, *Advanced Materials Technologies* **2018**, 3, 1800061.
- [25] G. Li, X. Wu, D.-W. Lee, *Sensors and Actuators B: Chemical* **2015**, 221, 1114.
- [26] G. Li, D.-W. Lee, *Lab on a Chip* **2017**, 17, 3415.
- [27] Y.-C. Sun, G. Boero, J. R. Brugger, *ACS Applied Electronic Materials* **2021**, 3, 5423.
- [28] L. Johnston, J. Yang, J. Han, K. Kalantar-Zadeh, J. Tang, *Journal of Materials Chemistry C* **2022**, 10, 921.
- [29] J.-H. Kim, S. Kim, H. Kim, S. Wooh, J. Cho, M. D. Dickey, J.-H. So, H.-J. Koo, *Nature Communications* **2022**, 13, 4763.
- [30] C. Xiao, J. Feng, H. Xu, R. Xu, T. Zhou, *ACS Applied Materials & Interfaces* **2022**, 14, 20000.
- [31] M.-G. Kim, D. K. Brown, O. Brand, *Nature Communications* **2020**, 11, 1002.
- [32] L. An, H. Jiang, D. de Camargo Branco, X. Liu, J. Xu, G. J. Cheng, *Matter* **2022**, 5, 1016.
- [33] W. Jung, G. R. Koirala, J. S. Lee, J. U. Kim, B. Park, Y. J. Jo, C. Jeong, H. Hong, K. Kwon, Y.-S. Ye, *ACS Nano* **2022**, 16, 21471.
- [34] R. F. Waters, P. A. Hobson, K. F. MacDonald, N. I. Zheludev, *Applied Physics Letters* **2015**, 107, 081102.
- [35] X. Miao, T. S. Luk, P. Q. Liu, *Advanced Materials* **2022**, 34, 2107950.
- [36] S. Datta, S. Vasini, X. Miao, P. Q. Liu, *Small Methods* **2024**, 8, 2400119.
- [37] J. Wang, S. Liu, S. Guruswamy, A. Nahata, *Optics Express* **2014**, 22, 4065.
- [38] W. Zhang, B. Zhang, X. Fang, K. Cheng, W. Chen, Z. Wang, D. Hong, M. Zhang, *Optics Express* **2021**, 29, 8786.
- [39] J. Wang, S. Liu, S. Guruswamy, A. Nahata, *Advanced Optical Materials* **2014**, 2, 663.
- [40] Q. H. Song, W. Zhu, P. Wu, W. Zhang, Q. Wu, J. Teng, Z. Shen, P. Chong, Q. Liang, Z. Yang, *APL Materials* **2017**, 5, 066103.
- [41] M. Losurdo, Y. Gutiérrez, A. Suvorova, M. M. Giangregorio, S. Rubanov, A. S. Brown, F. Moreno, *Advanced Materials* **2021**, 33, 2100500.
- [42] S. Catalán-Gómez, S. Garg, A. Redondo-Cubero, N. Gordillo, A. de Andrés, F. Nucciarelli, S. Kim, P. Kung, J. L. Pau, *Nanoscale Advances* **2019**, 1, 884.

- [43] S. Catalán-Gómez, C. Bran, M. Vázquez, L. Vázquez, J. Pau, A. Redondo-Cubero, *Scientific Reports* **2020**, 10, 1.
- [44] C.-Y. Chen, C.-Y. Chien, C.-M. Wang, R.-S. Lin, I.-C. Chen, *Materials* **2022**, 15, 2145.
- [45] M. W. Knight, T. Coenen, Y. Yang, B. J. Brenny, M. Losurdo, A. S. Brown, H. O. Everitt, A. Polman, *ACS Nano* **2015**, 9, 2049.
- [46] L. Martin-Monier, T. D. Gupta, W. Yan, S. Lacour, F. Sorin, *Advanced Functional Materials* **2021**, 31, 2006711.
- [47] A. Zavabeti, J. Z. Ou, B. J. Carey, N. Syed, R. Orrell-Trigg, E. L. Mayes, C. Xu, O. Kavehei, A. P. O'Mullane, R. B. Kaner, *Science* **2017**, 358, 332.
- [48] P. C. Wu, T.-H. Kim, A. S. Brown, M. Losurdo, G. Bruno, H. O. Everitt, *Applied Physics Letters* **2007**, 90, 103119.
- [49] S. Vivekchand, C. J. Engel, S. M. Lubin, M. G. Blaber, W. Zhou, J. Y. Suh, G. C. Schatz, T. W. Odom, *Nano letters* **2012**, 12, 4324.
- [50] S.-Y. Tang, D. R. G. Mitchell, Q. Zhao, D. Yuan, G. Yun, Y. Zhang, R. Qiao, Y. Lin, M. D. Dickey, W. Li, *Matter* **2019**, 1, 192.
- [51] A. Yamaguchi, Y. Mashima, T. Iyoda, *Angewandte Chemie International Edition* **2015**, 54, 12809.
- [52] I. J. Luxmoore, C. H. Gan, P. Q. Liu, F. Valmorra, P. Li, J. Faist, G. R. Nash, *ACS Photonics* **2014**, 1, 1151.
- [53] Y. Wang, Y. Xie, *Journal of Materials Chemistry A* **2024**, 12, 7396.
- [54] Y. Cui, F. Liang, Z. Yang, S. Xu, X. Zhao, Y. Ding, Z. Lin, J. Liu, *ACS Applied Materials and Interfaces* **2018**, 10, 9203.
- [55] Y. Cui, F. Liang, S. Xu, Y. Ding, Z. Lin, J. Liu, *Colloids and Surfaces A* **2019**, 569, 102.
- [56] G. Whyman, E. Bormashenko, T. Stein, *Chemical Physics Letters* **2008**, 450, 355.
- [57] W. Lin, W. Qiu, Y. Tuersun, X. Huang, S. Chu, *Advanced Materials Interfaces* **2021**, 8, 2100819.
- [58] N. Hussain, T. Scherer, C. Das, J. Heuer, R. Debastiani, P. Gumbsch, J. Aghassi-Hagmann, M. Hirtz, *Small* **2022**, 18, 2202987.

Deterministic Fabrication of Liquid Metal Nanopatterns for Nanophotonics Applications

*Md Abdul Kaium Khan, Yaoli Zhao, Shreyan Datta, Puspita Paul, Shoaib Vasini, Thomas Thundat, and Peter Q. Liu**

ToC figure



We demonstrated a simple, yet effective technique based on the selective wetting (reactive wetting) mechanism to fabricate large arrays of nanoscale patterns made of gallium-based liquid metals with precisely defined shapes, sizes and spatial distributions with ~ 100 nm resolution. Such liquid metal nanoscale patterns may find a broad range of applications in areas including nanophotonics and nanoelectronics.